Engineering Structures 176 (2018) 115–126

Contents lists available at ScienceDirect

Engineering Structures

journal homepage: www.elsevier.com/locate/engstruct

Direct measurement of building transient and residual drift using an optical sensor system

Floriana Petrone[a,*], David McCallen[a,b], Ian Buckle[b], Suiwen Wu[b]

[a] Energy Geosciences Division, Lawrence Berkeley National Laboratory, Berkeley, CA, USA
[b] Department of Civil and Environmental Engineering, University of Nevada, Reno, NV, USA

ABSTRACT

Interstory drift (ID) is a key response parameter for buildings subjected to lateral loads and is used to define performance-based limit states, allowable deformations and damage states in a number of seismic design codes and standards. An ability to rapidly and accurately measure both transient and residual ID during an earthquake would provide important observables for understanding the seismic demands and post-earthquake condition of a building. Accurate retrieval of ID from accelerometer-based instrumentation systems can be very challenging, if not impossible, as a result of instrumentation limitations and the post-processing associated with strong motion accelerometer data. This is particularly true for the case in which residual drifts occur during inelastic building response. In the study presented herein, a newly developed optical sensor system, designed specifically for directly measuring both transient and residual ID, was experimentally evaluated through shake table testing and computational simulations. The ability of the sensor to accurately measure ID is demonstrated and key operational considerations for sensor system deployment are examined through a model-based investigation.

1. Introduction

Current building seismic design continues to trend towards performance-based approaches which allow building owners to rationally select desired performance goals on a risk-informed basis. A number of modern earthquake design codes and standards for buildings and industrial facilities now define performance limit states [1] or deformation limits [2–6] in terms of ID, as summarized in Table 1. In addition, specifications for post-earthquake building condition assessments utilize residual drift as a measure of building damage states [7].

In the event of a major earthquake, having rapid post-earthquake knowledge of building drifts to evaluate exceedance of selected limit states and the corresponding potential for building damage would be particularly useful for informing post-earthquake assessments, and for making timely decisions on continuity of operations for critical facilities.

While effective at measuring band-limited accelerations, the determination of broad-band displacement measurements can be very challenging with traditional strong motion accelerometers. Trifunac et al. and Trifunac and Todorovska [8,9] have discussed the challenges in determining ground displacement during an earthquake as well as the related problem of measuring structural displacement. The processing of strong motion acceleration data through some form of high-pass filtering schema is often conflicted by the need to apply corrections that remove instrument drift and system noise, which simultaneously removes low frequency response data and permanent displacements that might have occurred in the building system. Other mechanical means of measuring drift such as string potentiometers, have also proven to be problematic as the mechanical changes associated with sag and creep of wire systems evolves over time. Skolnik and Wallace [10] provide a summary of the current and potential future methodologies for measuring ID, along with a review of advantages and disadvantages of each technique, by which it is noted that accurate and reliable measurement of transient ID remains a significant technical challenge.

Optical techniques have been investigated by a number of researchers [11–14], but as yet without the system level development necessary to enable broad transition into practice. For example, Chen et al. [13] proposed a technique that relies on a laser beam projected from ceiling to floor onto an arrangement of four position sensitive detectors, which yield a measure of ID in three directions. However, no experimental evidence of the system performance under dynamic loading and on realistic structures experiencing earthquake-induced displacements is provided. More recently, Islam et al. [14] have explored a laser-based technique to measure ID. It consists of a laser pointing at an inclined reflecting surface, in which the change of distance between the vertical laser source and the reflecting surface caused by the horizontal displacement of the floor is geometrically translated into ID. However, no solution to correcting for the effect of the rotation at the laser location is provided, which is recognized as a key issue in the photoelectric technologies proposed so far to measure ID [10].

* Corresponding author.
E-mail address: florianapetrone@lbl.gov (F. Petrone).

https://doi.org/10.1016/j.engstruct.2018.08.087
Received 25 April 2018; Received in revised form 27 July 2018; Accepted 26 August 2018
Available online 10 September 2018
0141-0296/ Published by Elsevier Ltd.

Table 1
Provisions for building peak interstory drift (PID) ratio and residual interstory drift (RID) ratio in selected codes and standards.

Specification	Standard	Drift Specifications			
Specification of performance limit states (drifts for steel moment frame example)	ASCE 43-05	*Limit State A* Large permanent distortion short of collapse *Significant Damage* PID 3.5%	*Limit State B* Moderate permanent distortion *Generally repairable damage* PID 2.5%	*Limit State C* Limited permanent distortion *Minimal damage* PID 1.0%	*Limit State D* Essentially elastic behavior *No damage* PID 0.5%
Specification of maximum allowable drift limits	ASCE 7-16	*Risk Category I or II* PID 2.5%		*Risk Category III* PID 2.0%	*Risk Category IV* PID 1.5%
	Eurocode EN 1998-1 (2004)	Buildings with non-structural elements that do not interfere with structural deformation PID 1.0%/v		Buildings having ductile non-structural elements PID 0.75%/v	Buildings having brittle non-structural elements PID 0.5%/v
	New Zealand Standard NZS – 1170.5 (2004)	Upper bound limit applicable to the ultimate limit state of all buildings, imposed to limit the probability of instability PID 2.5%			
	Tall Building Initiative (TBI) 2.01 (2017)	Drift limit to provide protection against nonstructural element damage and ensure permanent lateral displacement of the structure is negligible PID 0.5% Story transient drift from analyses not to exceed PID 3.0%			
	Chilean Standard NCh433.Of96 (1996)	Drift limit to control stiffness, torsional plan rotation and damage of nonstructural componentsPID 0.2% (when evaluated at the center of mass) + 0.1% (if evaluated at a point different from the center of mass)			
Specification of residual drift limits for post-earthquake structural assessments	FEMA P58-1 (2012)	*Damage State DS4* Residual drift is sufficiently large that the structure is in danger of collapse from aftershocks High ductility systems RID 4.0% Moderate ductility systems RID 2% Limited ductility systems RID 1%	*Damage State DS3* Major structural realignment is required to restore margin of safety for lateral stability RID 1.0%	*Damage State DS2* Realignment of structural frame and related structural repairs required to maintain permissible drift limits RID 0.5%	*Damage State DS1* No Structural realignment is necessary for structural stability RID 0.2%
	Tall Building Initiative (TBI) 2.01 (2017)	Residual drift to protect against excessive post-earthquake deformations that likely will cause condemnation or excessive downtime to perform repairs RID 1.0%			

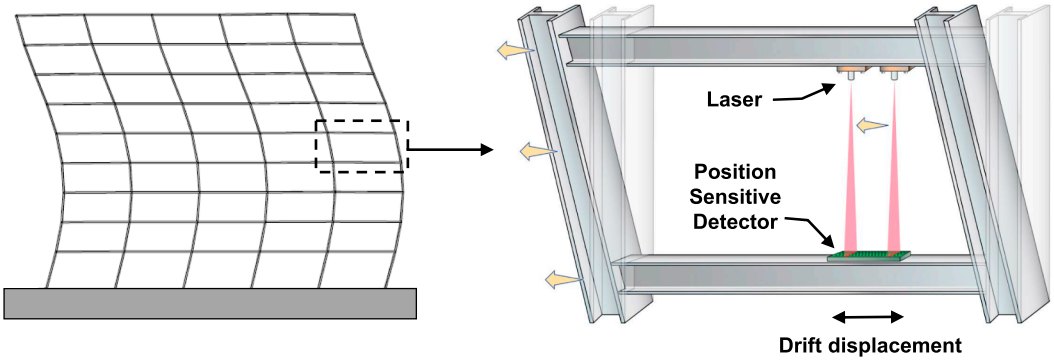

Fig. 1. Measurement of Interstory Drift with an optical sensor.

One optical concept for drift measurement relies on propagating laser light impinging on a Position Sensitive Detector (PSD) that can accurately measure the time-dependent point of incidence of the laser beam as indicated in Fig. 1. As story drift occurs, the laser translates on the PSD providing a direct measure of ID.

Recently, a new optical sensor concept for measuring ID, referred to as a Discrete Diode Position Sensor (DDPS), has been developed by McCallen et al. [15]. In static drift tests and small-scale laboratory dynamic tests, the DDPS has been demonstrated to be capable of accurately measuring both transient and residual ID [15]. In the study described herein, the design of the DDPS was advanced to a second-generation prototype that brings the system technology closer to being application-ready. The DDPS performance was tested under larger-scale, realistic earthquake test conditions and simulations of sensor system performance were performed to explore practical sensor mounting options for system optimization.

2. Advancement of the DDPS system

The underlying concept of the DDPS optical sensor is shown in

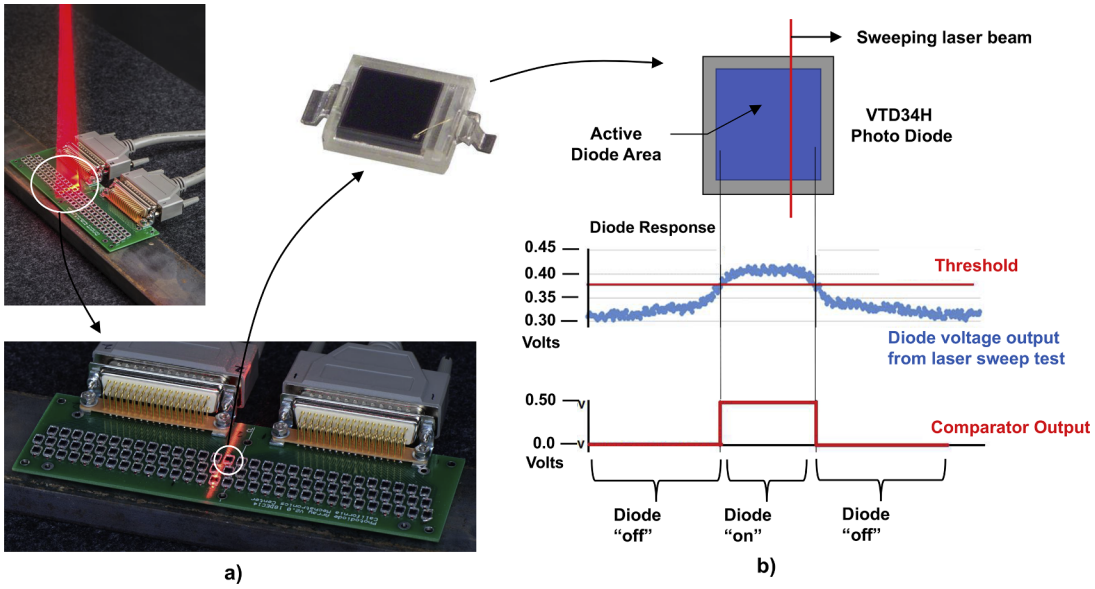

Fig. 2. Measurement principal of the DDPS. (a) Staggered diode array with incident laser light; (b) diode response test: voltage generated by a laser beam sweeping across a single diode and the corresponding output from the comparator circuit.

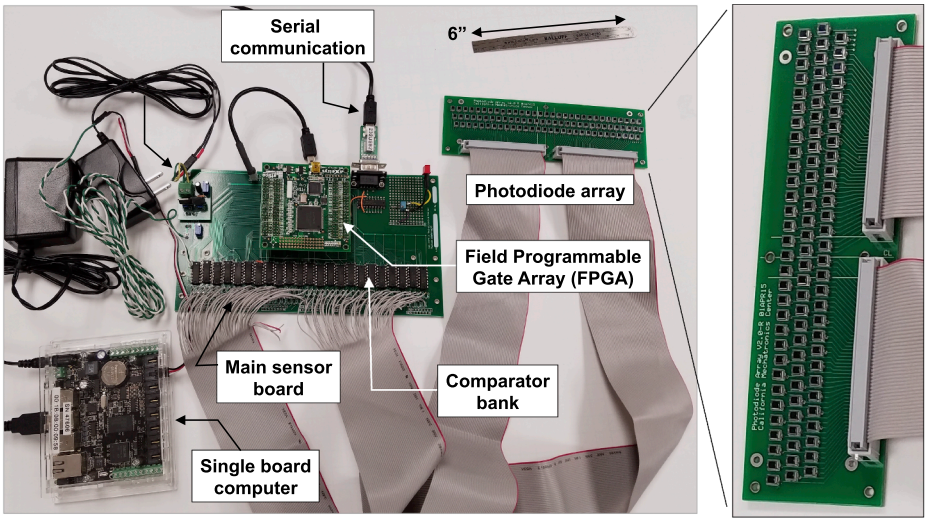

Fig. 3. First generation Discrete Diode Position Sensor with interconnected system components [14].

Fig. 2. A laser beam, diffracted by an optic to create a laser line source, is propagated across a building story height onto a staggered grid of light sensitive diodes that effectively serve as on/off switches. Each photodiode generates a voltage when contacted by incident laser light. By identifying which diodes in the array are actively being contacted by the incident light at any instant of time, the location of the laser line source is precisely determined as it moves across the sensor face during story drift. The first-generation DDPS sensor, as described and employed in [15], consisted of a set of inter-connected discrete hardware components, as shown in Fig. 3.

The DDPS was demonstrated capable of measuring the full dynamic waveforms of transient and residual drift, as illustrated in Fig. 4. While current standards specify requirements related to peak and residual drift ratio, consideration of full drift waveforms and the number of cycles at a given drift amplitude would provide a more rigorous definition of structural demands [16,17], especially for the evaluation of damage in structural and non-structural components. The ability to directly measure drift waveforms – transient interstory drift TID(t) – would enable such a demand measure.

In the current study, the sensor design has been advanced to a second-generation configuration where all components are mounted on a single custom circuit board as shown in Fig. 5. The DDPS is used to measure drift in the plane of a structural frame, and the diffracted beam line source is created with sufficient width to ensure it does not move off-sensor when out of plane displacements occur. The entire array of 92 diodes is sampled 384 times per second by a Field Programmable Gate Array (FPGA) that latches the output from a bank of comparators sampling the voltage generated by each diode to identify the instantaneous laser location. The output of the DDPS is a direct measure of interstory drift, which is stored in a microprocessor memory for local display or exfiltration to a centralized data acquisition system. The developed sensor technology could also be incorporated into advanced building monitoring frameworks such as described in Celebi et al. [18,19].

3. DDPS for building interstory drift measurements

The application of the DDPS technology for direct measurement of

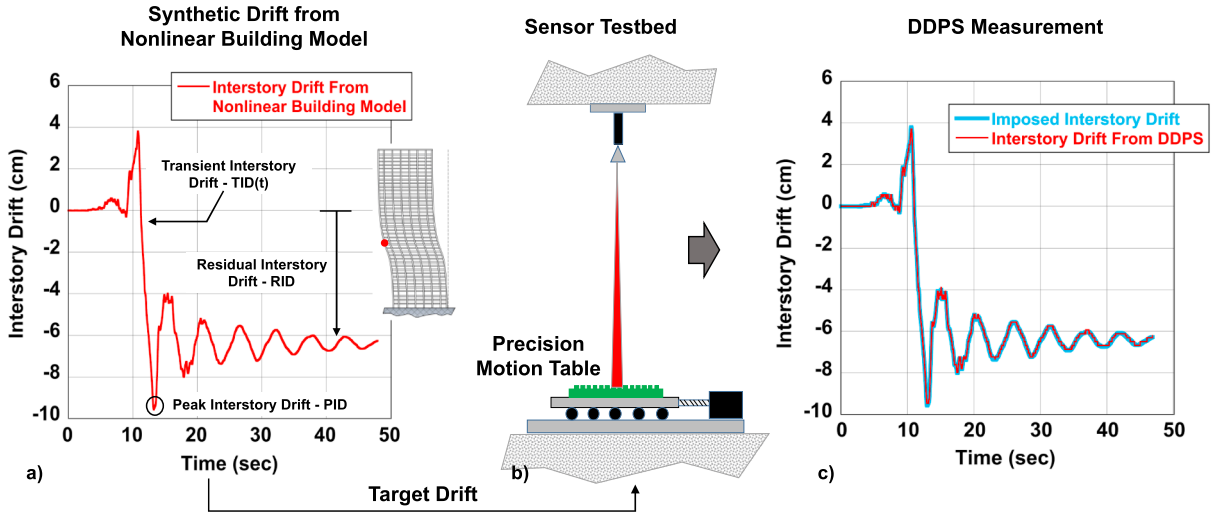

Fig. 4. TID(t), PID, RID: (a) Synthetic interstory drift history at the 13th floor (red dot) of a 40-story steel building under Landers Lucerne EW 1992 [17] defining the target motion; (b) DDPS testing on a precision motion table; (c) Imposed vs DDPS recorded interstory drift. (For interpretation of the references to colour in this figure legend, the reader is referred to the web version of this article.)

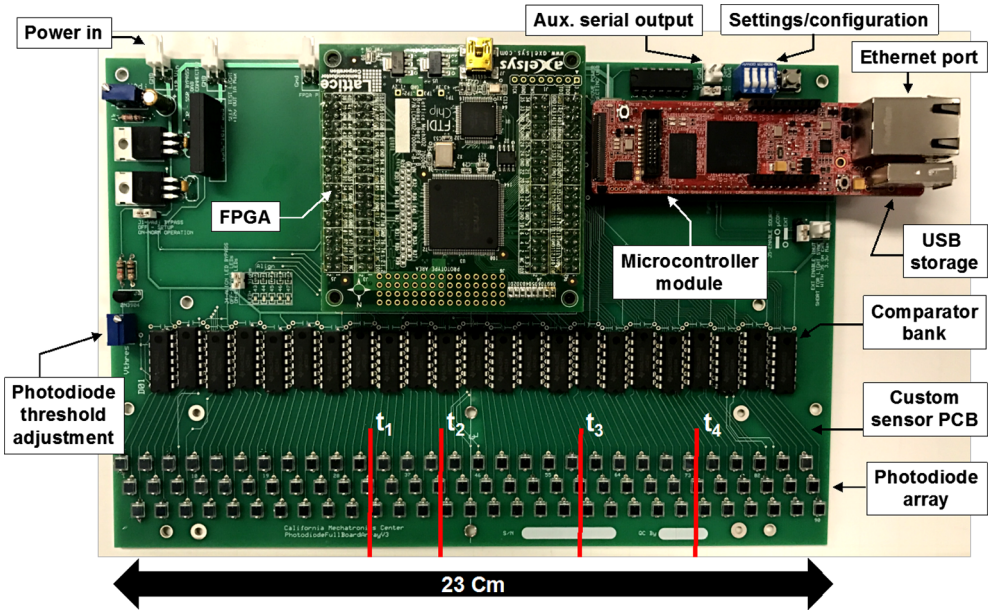

Fig. 5. Second generation Discrete Diode Position Sensor with single board mounted components (incident laser beam location illustrated at four instants of time).

building interstory drift must consider the local deformations of the structural members to which the sensor system components are mounted. As shown in Fig. 6, under lateral deformation the local rotation of the structural members at the point where the laser is mounted, $\Theta_{Laser}(t)$, can affect the location at which the laser beam impacts the DDPS. Previous studies have noted this issue [10,11,20,21] and a solution to address it has been proposed by McCallen et al. [15] through the combined use of a horizontally propagating laser beam and a vertical DDPS that together provide a measure of the local rotation, $\Theta_{Laser}(t)$.

From geometric considerations of the building frame deformed shape, the actual drift at each time step $\Delta_{Drift}(t)$ is computed as:

$$\Delta_{Drift}(t) = \Delta_{Observed}(t) + \Delta_{Rotation}(t) \quad (1)$$

where $\Delta_{Observed}(t)$ is the drift measured directly by the horizontal DDPS and $\Delta_{Rotation}(t)$ is the laser trace translation due to the local rotation at the laser mounting point, which in turn can be calculated as:

$$\Delta_{Rotation}(t) = \Theta_{Laser}(t) \cdot H \quad (2)$$

with $\Theta_{Laser}(t)$ representing the local rotation at the laser mount location and H the distance between the laser and the horizontal DDPS.

The unknown term of Eq. (2), $\Theta_{Laser}(t)$, is derived based on the measurements provided by a laser beam propagating onto the vertically mounted DDPS, as follows:

$$\Theta_{Laser}(t) = \Delta_{Vertical}(t)/W \quad (3)$$

where $\Delta_{Vertical}(t)$ is the vertical translation of the horizontally propagating laser beam measured on the vertical DDPS and W is the distance between the location of the vertically propagating laser and the vertical DDPS.

This methodology, consisting of utilizing a vertical laser beam impinging on a horizontal DDPS and a horizontal laser beam impinging on a vertical DDPS, provides a real-time measure of the actual interstory drift in a structure subjected to earthquake excitation. In practice, a simple optical splitter is used to divide a single laser beam into the vertical and horizontal line source beams necessary to trace the position on both the horizontal and vertical DDPS sensors as shown in Fig. 6.

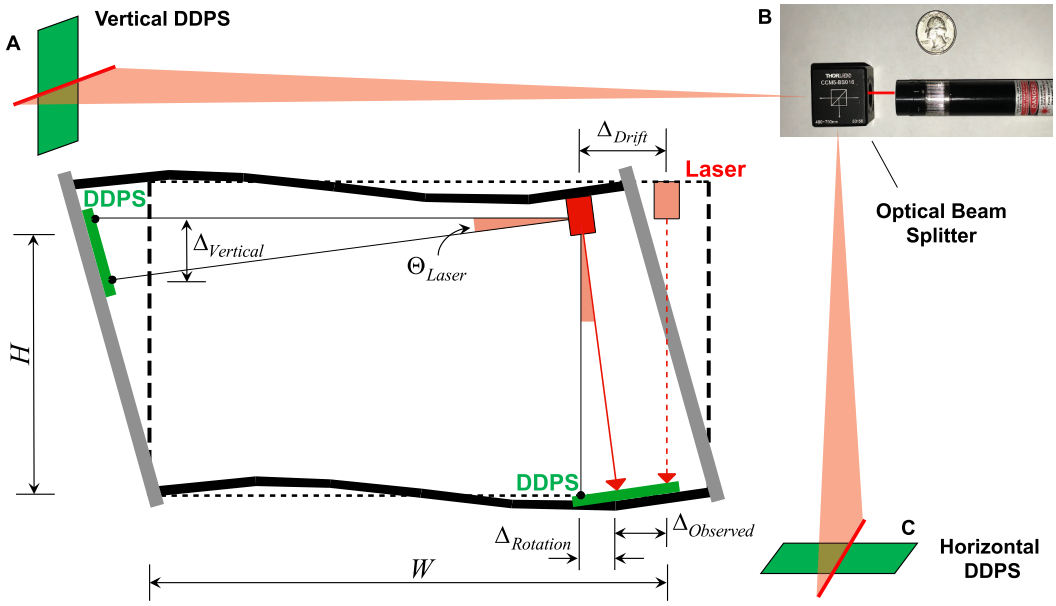

Fig. 6. Building frame deformed shape illustrating the local rotation, $\Theta_{Laser}(t)$, of a laser mounted on a horizontal beam and a vertically mounted DDPS to obtain local laser rotation.

4. Shake table experiments of sensor performance

The one-by-one bay, 1/3 scale, three-story steel frame shown in Fig. 7 was utilized for the experimental program. All beams in the EW direction and the third floor beams in the NS direction had rigid moment connections. Beams at the first and second floors in the NS direction had pinned connections. Intermediate, pinned connected struts located at each floor level in the EW direction provided support for floor mounted steel boxes where additional mass was placed to satisfy similitude requirements for inertial loads. This mass is summarized in Table 2, and details of the frame sections are given in Table 3.

The frame was mounted on a 50-ton, servo-hydraulic shake table in the Earthquake Engineering Laboratory of the University of Nevada, Reno (see Fig. 7), and a suite of diagnostics were installed to monitor displacements and accelerations in both horizontal directions. Ground truth measurements of the frame drift were obtained from 24 tensioned wires connected to string potentiometers to precisely track the change in distance between the two ends of the transducer, as illustrated in Fig. 8. Two sets of six wires were extended horizontally from the two diagnostic towers to the frame in the two horizontal directions, and an additional two sets of six wires were placed diagonally across each frame bay in the two directions. This arrangement provided two independent measurements of ID. The horizontal wires measured the absolute horizontal displacement at each floor level, which were

Table 2
Frame additional mass distribution.

	First Floor	Second Floor	Third Floor
Mass [kg]	7973	8318	6857

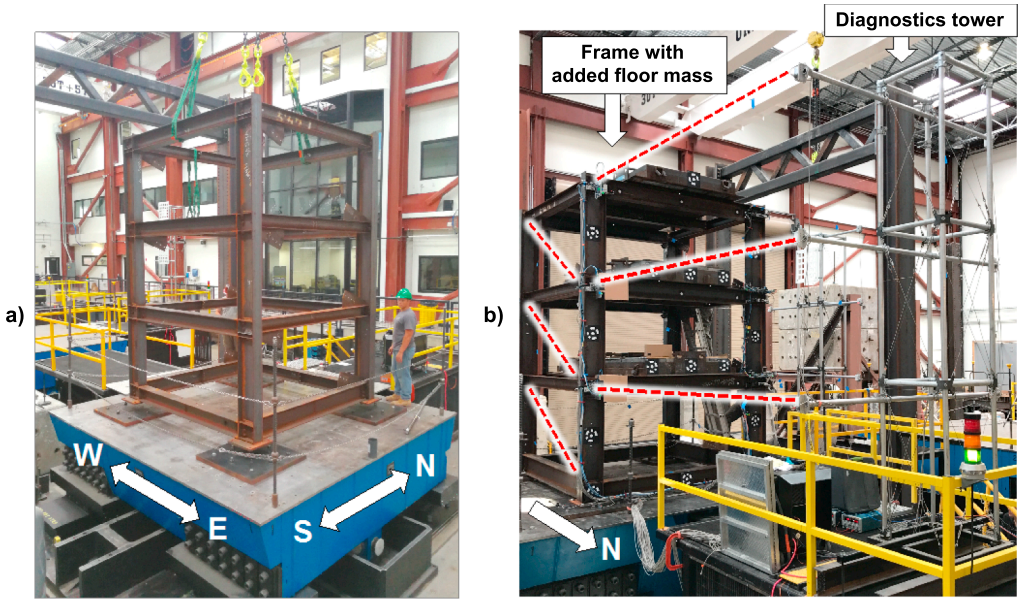

Fig. 7. One-third scale steel building. (a) Frame mounting on shake table; (b) frame with added floor mass and diagnostics (string potentiometers with tensioned wires indicated by red dashed lines). (For interpretation of the references to colour in this figure legend, the reader is referred to the web version of this article.)

Table 3
Steel Frame: cross-section properties of all members.

		Base	First Floor	Second Floor	Third Floor
Primary Beams	NS direction	W10 × 26	W6 × 15*	W6 × 15*	W6 × 15
	EW direction	W8 × 24	W8 × 24	W8 × 24	W8 × 24
Intermediate Trusses	EW direction	–	W6 × 15	W6 × 15	W6 × 15
Columns		–	W10 × 26	W10 × 26	W10 × 26

* Pinned connection.

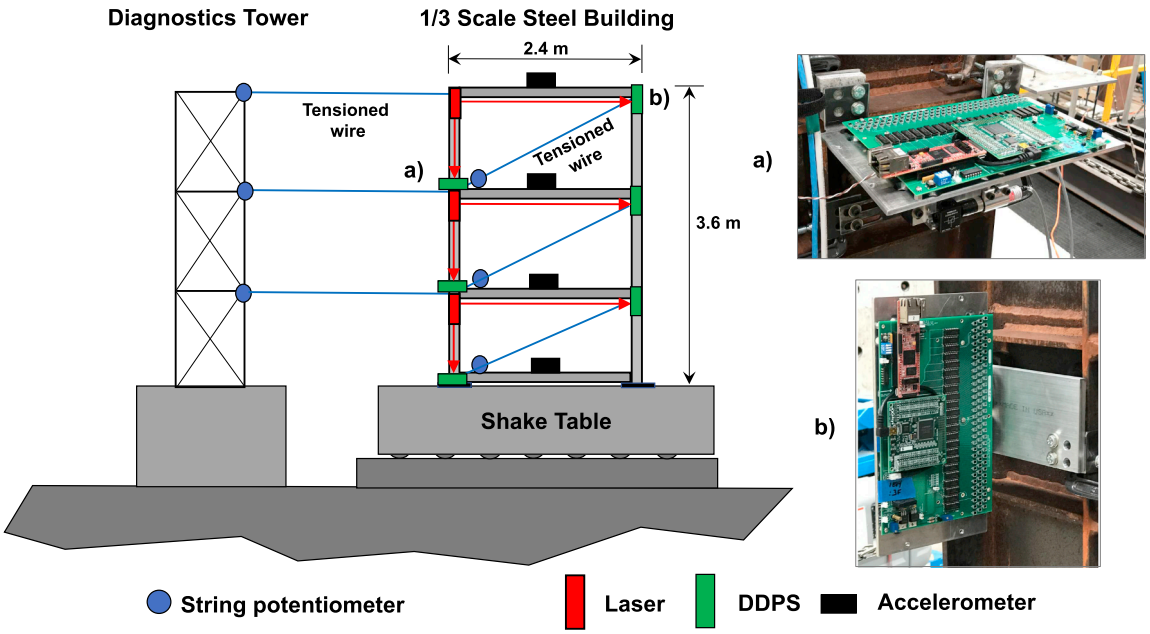

Fig. 8. Sensor system layout and diagnostic suite on the test frame.

differenced to obtain drift at each floor. The diagonal wires were used to measure the extension or contraction of the diagonal dimension of each frame bay, which was geometrically translated into interstory drift. The drift measurements recorded by both techniques were in good agreement, providing confidence in the ground truth floor drift measurements adopted as the benchmark for evaluation of the DDPS accuracy.

A total of six lasers and diffraction optics that split and diffract a single beam source into both vertical and horizontal directions, and twelve DDPSs were deployed on the frame to measure lateral displacements and the rotation at the mounting point of the lasers in both frame directions. The horizontal DDPS measures the bay horizontal translation relative to the floor below and the vertical DDPS provides laser rotation measurement. In addition, eight MEM326 accelerometers with a sampling frequency of 512 Hz were placed at the mid-span of all beams to measure the accelerations at each floor in both horizontal directions. Details of DDPSs and accelerometers deployment can be found in Fig. 8.

The experimental program consisted of a sequence of shake table tests. The testing approach began with scaled-down, low amplitude earthquake motions and was incrementally increased until full actual earthquake records, as well as some scaled-up motions, were achieved. Overall 30 earthquake tests were executed in succession at varying amplitudes for both uniaxial and biaxial motions. Two measured earthquake ground motion accelerations from two representative earthquakes were used: the 1940 El Centro California earthquake (El Centro station motion) and the 1994 Northridge California earthquake (Rinaldi station motion) [22]. The first record is representative of a ground motion in the far-field, while the latter of a ground motion in the near-field of the causative fault where low-frequency, near-fault waveforms are significant. The two measured horizontal components of motion for these earthquakes were applied biaxially in orthogonal directions to the test frame.

The fundamental objective was to assess the performance of the second generation DDPS at a more realistic scale associated with the 1/3 scale steel frame. Additionally, practical considerations of sensor performance under strong shaking and sensor mounting integrity were explored to ensure there was no unanticipated detrimental impact of strong shaking on sensor reliability or accuracy. Three representative datasets are shown in Fig. 9, comparing the total corrected drift obtained from the DDPS, see Eq. (1), with the ground truth drift measured by the string potentiometers.

For all three earthquake ground motions, the DDPS measurements corrected for laser rotation exhibited excellent agreement with the string potentiometer measurements. As indicated in Fig. 10, the maximum difference in measured drift was on the order of 2 mm, and both the amplitude and frequency content of the ID waveforms was well represented by the DDPS system. This was the same order of measurement error observed in previous DDPS testing (Fig. 4), which demonstrates that the error is independent of drift amplitude. Additional comments about theoretical sensor position measurement errors can be found in [15].

Although the principal function of the DDPS is to provide direct measurements of interstory drift, an additional application of the DDPS system could allow estimating in-structure absolute accelerations. By deploying a DDPS at each floor, the displacement at each floor relative to the base of the building can be computed by a summation over all lower floors, that is

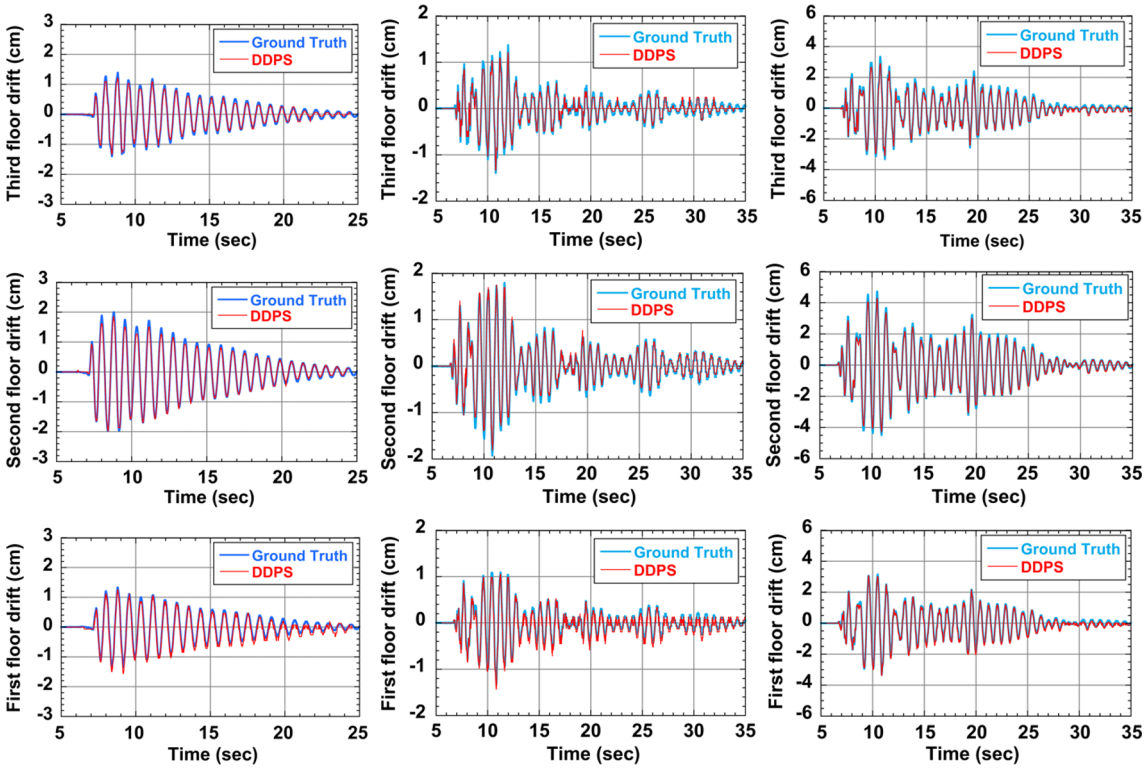

Fig. 9. Ground truth vs DDPS measurements of interstory drift at all three floors for 1994 Rinaldi-scaled by factor 0.2 (left), 1940 El Centro (middle) and 1940 El Centro-scaled by factor 2.5 (right).

$$D_i(t) = \sum_{k=1}^{i} d_k(t) \tag{4}$$

where $D_i(t)$ is the displacement of floor i (with $k = 1, 2...i$) at time t relative to the base of the building and $d_k(t)$ is the interstory drift displacement of story k at time t as measured by the DDPS. Eq. (4) can be used to calculate relative story acceleration by double differentiation of the relative displacements and, once the ground acceleration is

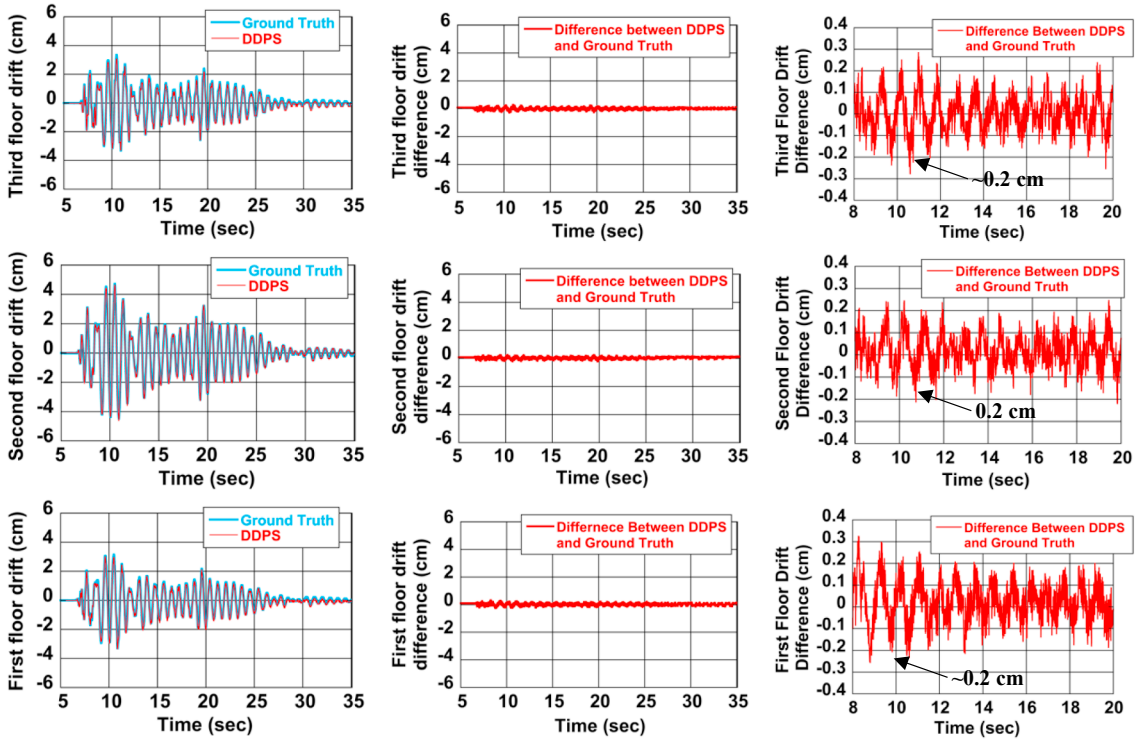

Fig. 10. Sensor measurement error for 1940 El Centro-scaled by factor 2.5: ground truth vs DDPS measurements of interstory drift at all three floors (left), measurement error (middle) and detail of the measurement error (right).

known (for example through the deployment of a free field strong motion accelerometer), to calculate the absolute story acceleration. As discussed in [15], the quantized (piecewise step function) nature of the DDPS measurement from the laser transitioning incrementally across diodes can result in fictitious high frequency content when the drift response histories are differentiated. To mitigate fictitious high frequency, the drift waveform must be processed to remove the effects of the small displacement step-functions. In the current study, the ability of the DDPS system to provide a reliable estimate of the in-structure absolute accelerations was evaluated by comparison with the accelerations recorded by the accelerometers mounted on the test frame. Utilizing Eq. (4), the absolute displacement history at each floor was calculated by adding the known shake table displacement to the relative displacement history measured by the DDPS at each floor level. The quantized floor absolute displacement histories were then low-passed with a Butterworth filter using a cutoff frequency of 10 Hz and double-differentiated to obtain absolute floor accelerations. A comparison between the in-structure absolute accelerations directly measured by the accelerometers and those derived from DDPS data, expressed in terms of in-structure acceleration spectra at all three floors, is shown in Fig. 11.

The good agreement of the spectral accelerations around the fundamental frequency of the structure (~0.77 s) demonstrates the potential of the DDPS to be used to derive in-structure accelerations that are useful for the interpretation of inertial loads and equipment loads. Spectral frequency content is matched at lower frequencies, but at higher frequencies amplitude differences are observed (i.e. ~10 Hz), where the DDPS results for this very stiff test structure are sensitive to the signal processing employed in smoothing the quantized displacement histories recorded by the DDPS.

5. Model-based simulation of sensor system performance

To further assess the sensor system performance and examine the potential of a numerical model to serve as a predictive tool to guide DDPS system design, a detailed three-dimensional finite element model (FEM) of the frame was developed in the OpenSees environment [23]. Displacement-based beam elements with fiber cross sections including multiple integration points were employed to model primary beams and columns, whereas truss-elements were adopted for the intermediate struts supporting the floor masses. Pinned-connections of the beams at the first and second floor in the weak direction, see Fig. 7, were modeled with multi-point constraints between nodes. The discretization at both the element and cross-section level was determined based upon a sensitivity analysis, whereby each element was subdivided into 4 beam-elements along the length and each cross-section was discretized into 40 fibers. Each fiber was assigned a uniaxial bilinear steel material object (Steel01), with Young's modulus equal to 200,000 MPa and yield strength equal to 344.74 MPa. A consistent mass matrix was generated for the bare frame through the definition of geometry and material mass density, whereas the additional mass placed at each floor was represented by lumped masses at model nodes.

In the course of the modeling effort it was discovered that the model predictions for the test frame with pinned connected joints were very sensitive to specific model parameters, such as frame damping and frame mass. To achieve the greatest accuracy possible with the frame model, two approaches were examined for calibrating the model with as-built structural parameters.

First, to evaluate the frame dynamics under small amplitude vibrations, a snap test, consisting of a sudden, short-duration displacement of the shake table was employed. The snap test provides an impulse type excitation to the structure and the ring-down observed during free vibration was used to identify both the fundamental natural frequency of the frame as well as the frame's inherent damping. Displacements at the third floor were recorded with the string potentiometers and the logarithmic decrement was used to compute the corresponding damping (assuming the frame was viscously damped) [24]. The effective damping was calculated as the average of the first five and second five peaks of the ring-down, yielding a damping ratio of 2.5%.

Secondly, to account for potential changes in the frame dynamics under strong motion records and to obtain a confirmation of the total active mass in the system, which was hand calculated for the baseline FEM, the frame model employing the initial damping of 2.5% was evaluated in the UQFEM environment [25]. This evaluation utilized the frame response to the Rinaldi strong motions. The UQFEM structural identification routine adopts a nonlinear interior point full-Newton optimizer from the OPT++ library [26,27], and provided optimized values for the frame damping ratio and the mass, which resulted in a decrease of the damping ratio to 1.5% and an increase of the total mass by 1.8% for obtaining best-fit to the Rinaldi motion data. It was clear from the analyses of a number of earthquake motions and from finite element simulations that the frame damping actually decreased under higher amplitude excitations. It is speculated that the pinned connections in the frame dissipated less energy at higher amplitudes of vibration. For the final model, Rayleigh damping was adopted with a 1.5% damping ratio anchored to the first and second modes of the frame in the weak direction.

The FEM was statically initialized under gravity loads and then subjected to the same sequence of earthquake ground motions followed

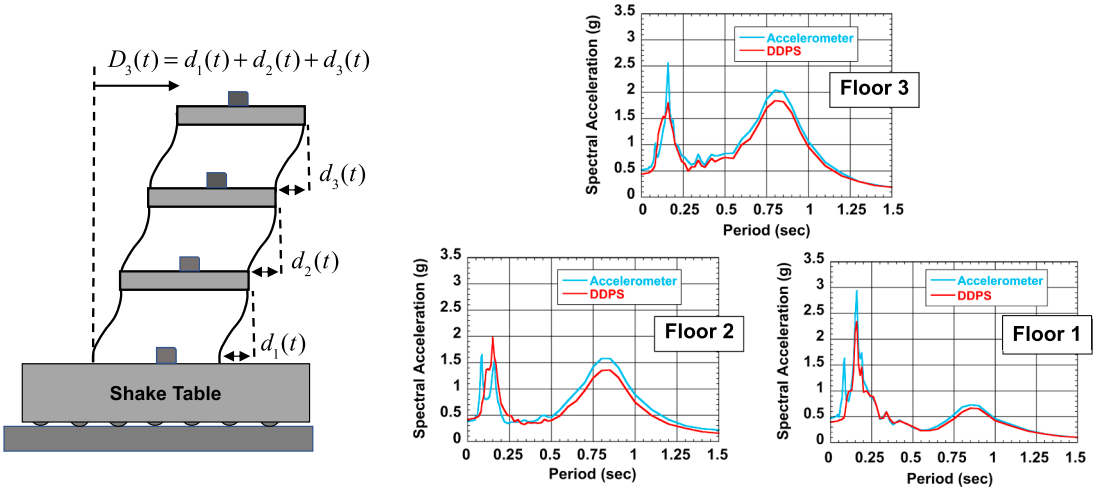

Fig. 11. In-structure response spectra at all three floors: accelerometer direct measurements vs double-differentiated and low-pass filtered DDPS data.

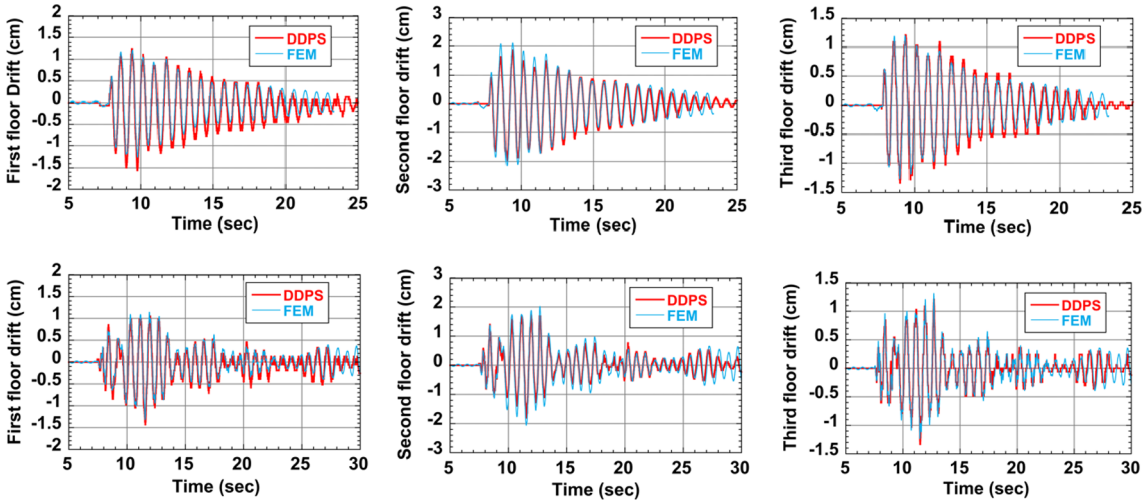

Fig. 12. DDPS measured drift vs FEM computed drift in NS direction at all three floors for bidirectional 1994 Northridge Rinaldi (scale factor 0.2) (top) and bidirectional 1940 El Centro (bottom).

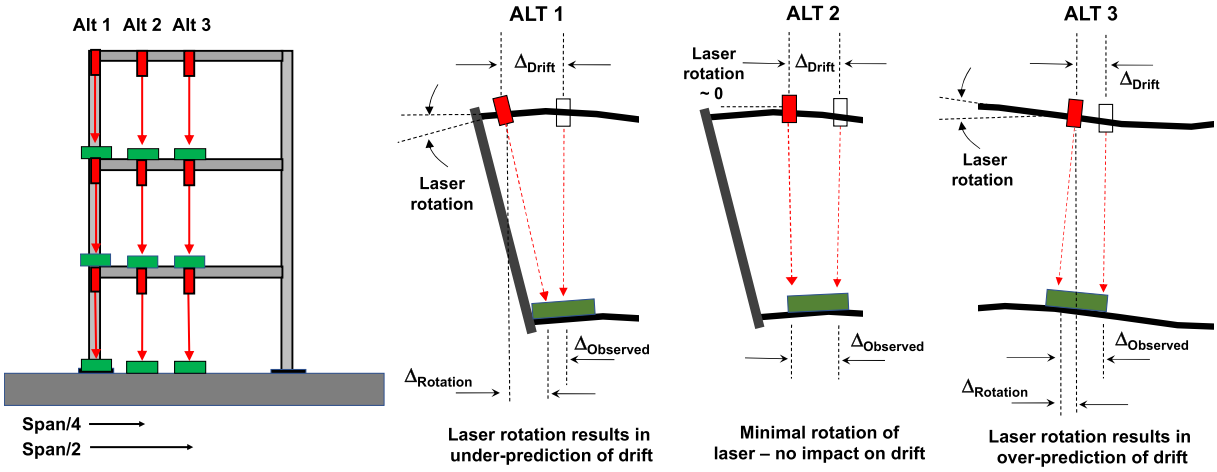

Fig. 13. Deployment of vertical lasers and horizontal DDPSs at the structural joint (ALT1), at 1/4 of the beam span (ALT2) and at beam mid-span (ALT3) and detail of the corresponding laser rotations.

in the experimental program. The approach was to perform a response simulation and employ the model predicted displacements and rotations at the laser and sensor mount locations to compute the expected measurements of the sensor system. The objective was twofold: first, to evaluate the ability of the model to capture the response of the as-built tested frame and second, to demonstrate the potential to develop a simulation-based predictive tool to analyze and design a DDPS system.

The responses under the 1940 El Centro California bidirectional motion and the 1994 Northridge California earthquake Rinaldi bidirectional motion, the latter scaled by a factor of 0.20, are shown in Fig. 12. The comparison between the DDPS measurements and the simulated sensor performance is expressed in terms of interstory drift histories at all floors.

The computational model yielded accurate predictions of the interstory drift waveforms measured by the DDPSs. The observed agreement provides validation of the numerical model against experimental data, and demonstrates the ability of the displacements and rotations obtained from a simulation model to accurately estimate the DDPS performance.

6. Computational investigation of DDPS system mounting options

The experimental work performed has illustrated the potential sensitivity of the DDPS system performance to the specific manner in which the system components are mounted to the structure being monitored. For practical application, it will be essential to both understand and optimize the DDPS sensor system mounting approach, and provide clear guidance for sensor system deployment. For many structures, the requirement for including a horizontal line of sight to measure laser rotation would add operational complexity and cost to a DDPS system deployment. System simulations were developed to investigate alternative deployment and mounting configurations, with an objective of evaluating the potential for eliminating the need for laser rotation measurements and significantly reducing the number of lasers and sensors required at each floor. The numerical investigation on alternative DDPS system mounting solutions was conducted on a substructure extracted from the experimental 1/3 scale steel frame, idealized as a pure planar moment frame with moment connections.

The first portion of the simulations explored the implications of mounting the vertical laser at different locations along the span of a horizontal beam. The approach was to simulate the horizontal DDPS measurements without rotation correction and compare the interstory drift obtained from the simulation-based DDPS readings with the interstory drift calculated based on the FEM transient response.

Three alternative cases were analyzed, in which the DDPS system, consisting only of a vertical laser and horizontal sensor, was placed at the beam-column joint (ALT 1), at ¼ of the beam span (ALT 2) and at the beam mid-span (ALT 3) at each floor, as illustrated in Fig. 13.

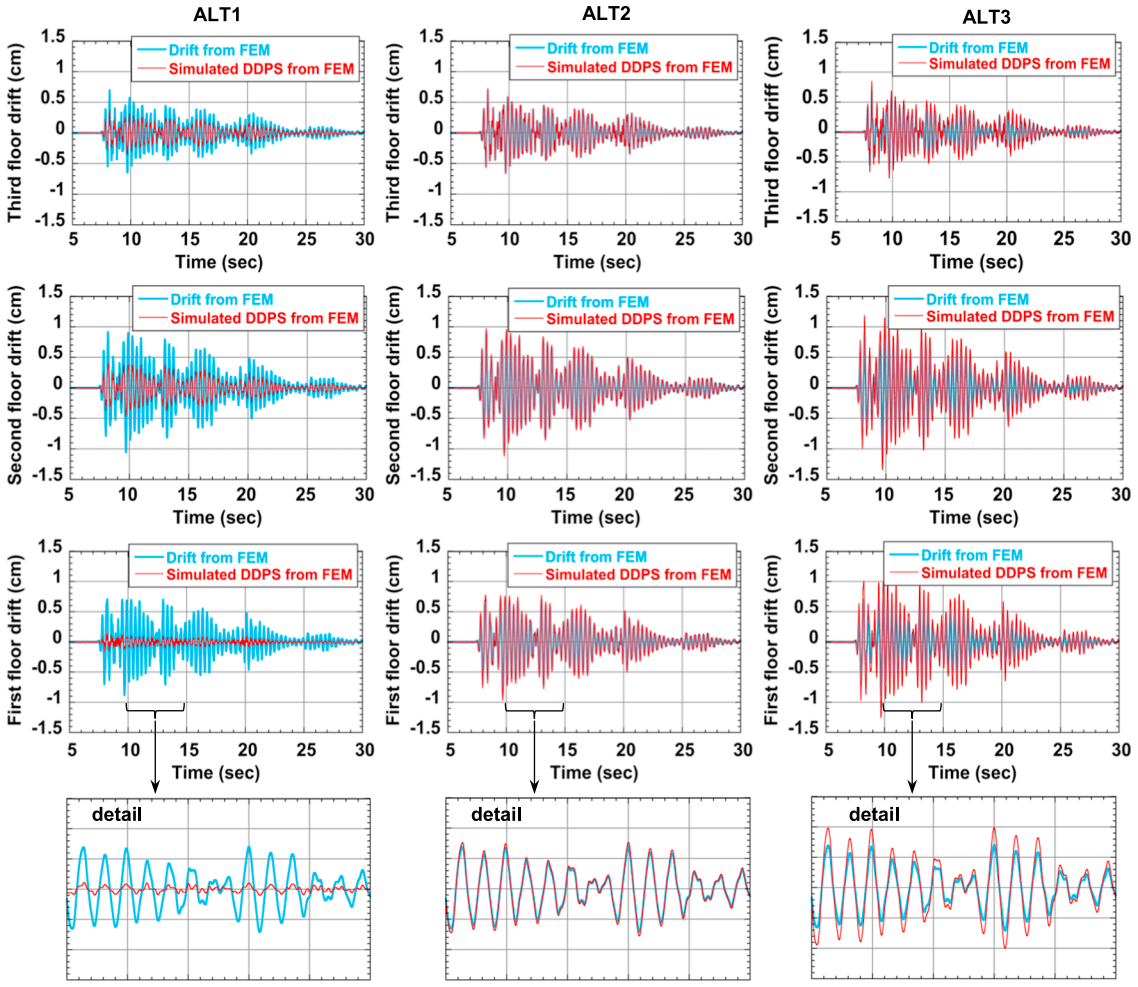

Fig. 14. FEM-based DDPS interstory drift measurements (without rotation correction) vs FEM interstory drift for DDPS placed at the structural joint (left), ¼ of the beam span (middle) and at the beam mid-span (right) at all three floors.

The planar frame model was subjected to the uniaxial 1940 El Centro input motion and Fig. 14 shows the simulation-based DDPS interstory drift measurements for all three mounting configurations compared with the numerically computed interstory drift history at all three floors. By geometrically interpreting the effect of rotation for each mounting location from an exaggerated graphic of the frame FEM output, see Fig. 13, it is observed that the DDPS sensor measurement for ALT1 (i.e. the sensor measurement uncorrected for laser rotation) should tend to under-predict the actual drift. For ALT2, the laser should translate through vertical motion with no local rotation, meaning that the direct, uncorrected, sensor measurement yields a good representation of drift. Finally, for ALT3 the geometric deformation indicates that the direct, uncorrected sensor measurement should tend to overestimate the actual drift.

The FEM results for the sensor performance for ALT1-ALT3 without rotation correction are shown in Fig. 14. The trends in the simulated sensor error are in direct correlation with the geometric interpretations of Fig. 13.

From these observations of the beam kinematics and simulations, a mounting option such as ALT 2 could provide a solution that minimizes the number of sensors to deploy at each floor. In practice, the ALT 2 mounting location will have some initial finite, small rotation due to structural dead loads, but the laser will typically be mounted to the deformed shape to be vertically aligned after gravity deformations occur. The benefits of such a mounting could be substantial and the practicality of realized sensor performance should be explored in future experimental tests.

A second type of laser mounting option which could have significant practical deployment benefits was numerically explored. This option consisted of mounting the laser to a pinned-pinned strut that would serve to isolate the laser from local rotations of the main structure, as shown in Fig. 15. The planar frame FEM was augmented with a pin-connected strut at each floor to evaluate this mounting option. Under this arrangement the laser rotation is only associated with the rigid-body strut rotation resulting from column lengthening and shortening under lateral frame displacement.

Following the same approach adopted for the previous mounting system evaluation, the structure was initialized under gravity loads and then subjected to uniaxial 1940 El Centro input motion. The DDPS response without rotation correction was simulated under the hypothesis that the vertical lasers were mounted at mid-span of the pinned struts and included the small rigid body rotations that occur in the struts when the structure displaces laterally.

Fig. 15 shows the comparison between the simulated DDPS interstory drift measurements from FEM and the FEM computed interstory drift at all three floors. The excellent agreement of the drift response history demonstrates the potential for developing a DDPS system that adopts just one vertical laser and one horizontal sensor at each floor. This approach could facilitate the DDPS system mounting on existing structures and would be applicable across multiple structure types (i.e. moment frames, braced frames, shear wall structures).

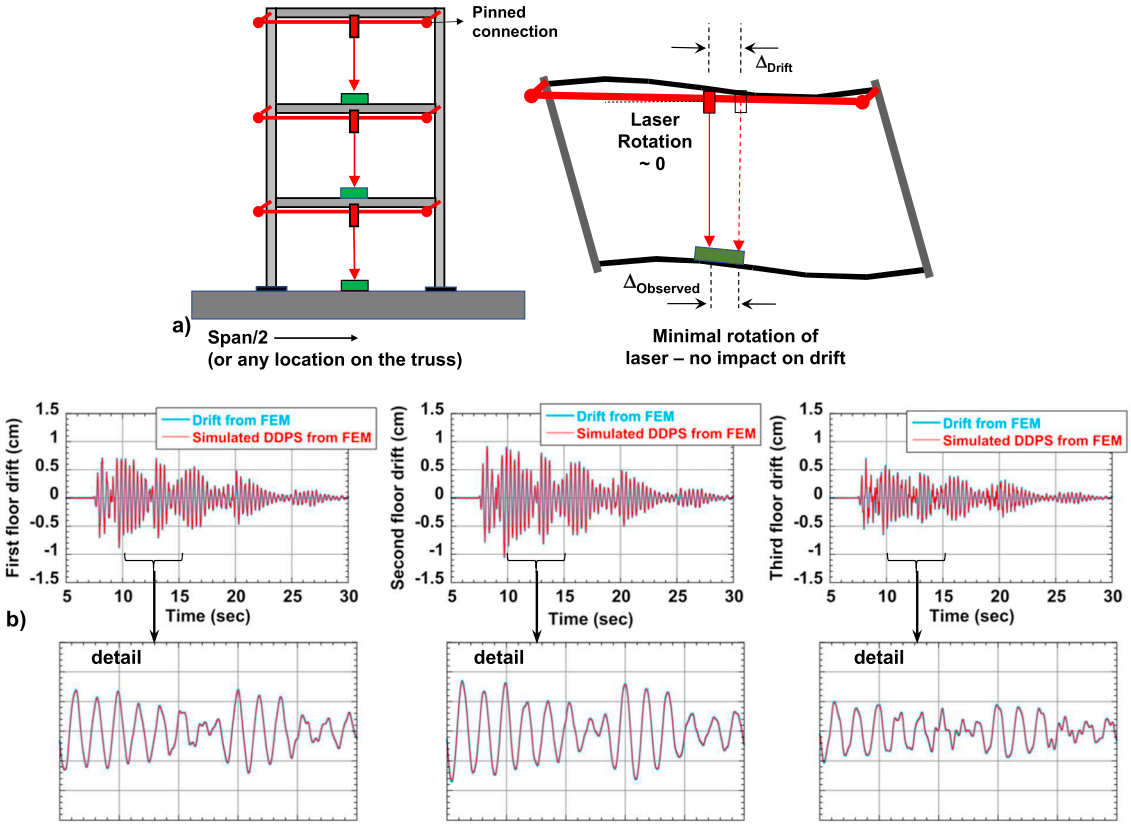

Fig. 15. Deployment of vertical lasers at the mid-span of pinned-pinned struts: (a) Strut configuration and (b) FEM-based DDPS interstory drift measurements (without rotation correction) vs FEM interstory drift for DDPS placed at the mid-span of pinned-pinned struts at all three floors.

7. Discussion

In this study, the design of the DDPS system successfully progressed towards a single board prototype configuration that brings the technology closer to an application-ready status. The performance of the second-generation sensors was verified by comparison with experimental data under more realistic test conditions (e.g. a larger structure, stronger motions) and important practical considerations for sensor system mounting and deployment were explored. By carefully selecting the position of the laser mounting location, or through the deployment of a mounting strut that isolates the laser from local member rotations, it appears from numerical simulations that the need to measure and correct for local rotations can be eliminated. This has important implications for both the practicality and cost of sensor deployments on actual buildings and should be rigorously verified in future system experimental testing.

In the testing campaign that was conducted, the shake table tests were run sequentially. This is much like what might occur in an actual strong earthquake with a sequence of multiple aftershocks, and there was no indication of any damage or adverse impact on the performance of the DDPS. The response of the scaled frame to 250% of El Centro motions was extreme and all sensors performed without fault or degradation.

Moving forward, additional value engineering should occur to optimize the single-board sensor design. The footprint of the sensor package can be further reduced through vertical stacking and implementation of new hardware technology can move towards an optimal cost function (e.g. replacement of the current comparator bank with a single multiple-channel comparator chip). Additional developments are under consideration, such as the augmentation of the current wire-connected power source with a battery back-up that would keep the monitoring system operative in the event of a power outage after a major earthquake event. A wireless communication capability for data exfiltration would also be an important feature for enabling sensor system deployment. In addition, an experimental test that includes significant inelastic, permanent drifts in the test structure should be used to further verify the ability to measure RID in a representative test structure.

The optical sensor system offers the potential of uniquely measuring, in real time, transient interstory drift waveforms, peak interstory drift at any point in the earthquake response, and residual drift due to inelastic structural deformation. This can provide engineers and facility owners with a powerful new tool for measuring building response and rapidly informing post-earthquake decisions and actions.

Acknowledgements

This work was supported by the U.S. Department of Energy, Office of Nuclear Safety Research and Development Program (NSRD). The support and encouragement of NSRD program manager Dr. Alan Levin is greatly appreciated. The DDPSs were fabricated at California State University Chico by engineers Jason Coates and Nicholas Repanich, whose contribution is gratefully acknowledged. Further, the support of Dr. Patrick Laplace, Chad Lyttle and Todd Lyttle of the University of Nevada Center for Civil Engineering Earthquake Research was crucial to the experimental campaign and the authors are grateful for their expert contributions.

References

[1] American Society of Civil Engineers (ASCE). Seismic design criteria for structures, systems, and components in nuclear facilities. Reston (VA): ASCE/SEI 43–05; 2005.
[2] American Society of Civil Engineers (ASCE). Minimum design loads and associated criteria for buildings and other structures. Reston (VA): ASCE/SEI-7; 2016.
[3] European Committee for Standardization (CEN). Eurocode 8: Design of structures for earthquake resistance – Part 1: General rules, seismic actions and rules for buildings. European Committee for Standardization; 2004.

[4] Standards New Zealand. Structural design actions – Part 5: Earthquake actions. New Zealand: NZS 1170-5; 2004.
[5] Pacific Earthquake Engineering Center (PEER). Tall buildings initiative (TBI) - guidelines for performance-based seismic design of tall buildings PEER report 2017/06 Berkeley: University of California; 2017
[6] Instituto Nacional de Normalizacion – INN-Chile. Chilean Standard NCh 433.Of96: Seismic Design of Buildings; 1996.
[7] Applied Technology Council. Seismic performance assessment of buildings – Volume 1 – Methodology – FEMA P-58-1, September 2012, Redwood City, California 94065; 2012.
[8] Trifunac MD, Ivanovic SS, Todorovska MI. Apparent periods of a building II: Time-frequency analysis. J Struct Eng 2001;127:527–37.
[9] Trifunac MD, Todorovska MI. A note on the usable dynamic range of accelerographs recording translation. J Soil Dyn Earthq Eng 2001;21:275–86.
[10] Skolnik DA, Wallace JW. Critical assessment of interstory drift measurements. J Struct Eng 2010;136:1574–84.
[11] Bennett KD, Batroney CB. Interstory drift monitoring in smart buildings using laser crosshair projection. Opt Eng 1997;36:1889–92.
[12] Yun F, Yong Z, Weimin C, Rong S, Shanglian H, Bennett KD. Five dimensional interstory drift measurement with cross hair laser. Acta Photon Sin 1999;28(11):1006–9.
[13] Chen WM, Bennett KD, Feng J, Wang YP, Huang SL. Laser technique for measuring three dimensional interstory drift. Proc Soc Photon Opt 1998;3555:305–10.
[14] Islam MN, Zareie S, Shahria Alam M, Seethaler RJ. Novel method for interstory drift measurement of building frames using laser-displacement sensors. J Struct Eng 2016;142(6):06016001.
[15] McCallen D, Petrone F, Coates J, Repanich N. A laser-based optical sensor for broadband measurements of building earthquake drift. Earthq Spectra 2017;33(4):1573–98.
[16] Barbosa AR, Ribeiro FLA, Neves LAC. Influence of earthquake ground-motion duration on damage estimation: application to steel moment resisting frames. Earthq Eng Struct Dyn 2017;46:27–49.
[17] Hancock Jonathan, Bommer Julian J. A state-of-knowledge review of the influence of strong-motion duration on structural damage. Earthq Spectra 2006;22(3):827–45.
[18] Çelebi M, Sanli A. GPS in pioneering dynamic monitoring of long-period structures. Earthq Spectra J EERI 2002;18(1):47–61.
[19] Çelebi M, Sanli A, Sinclair M, Gallant S, Radulescu D. Real-time seismic monitoring needs of a building owner – and the solution: a cooperative effort. Earthq Spectra 2004;20(2):333–46.
[20] Chen X. Near-field ground motion from the landers earthquake Report no EERL 95-02 Pasadena (California, USA): California Institute of Technology, Earthquake Engineering Research Laboratory; 1995.
[21] Skolnik DA, Kaiser WJ, Wallace JW. Instrumentation for structural health monitoring: measuring interstory drift. Proceedings of the 14th world conference on earthquake engineering, 12–17 October, Beijing, China 2008.
[22] Pacific Earthquake Engineering Research Center Ground Motion Database (PEER). http://ngawest2.berkeley.edu/.
[23] OpenSees v 2.5.0 [Computer software]. Berkeley (CA): Pacific Earthquake Engineering Research Center, Univ. of California.
[24] Chopra AK. Dynamics of structures: theory and application to earthquake engineering. 4th ed. Upper Saddle River (NJ): Prentice Hall; 2012.
[25] UQFEM Application. SIMCenter, computational modeling and simulation center. https://simcenter.designsafe-ci.org/research-tools/uqfem-application/.
[26] Adams BM, et al. DAKOTA, a multilevel parallel object-oriented framework for design optimization, parameter estimation, uncertainty quantification, and sensitivity analysis: version 6.7 user's manual. Albuquerque (NM, USA): Sandia National Laboratories; 2009.
[27] Meza C, Oliva RA, Hough PD, Williams PJ. OPT++: an object oriented toolkit for nonlinear optimization. ACM Trans Math Softw 2007;33(2).